AIAA JOURNAL
Vol. 45, No. 6, June 2007

Inverse Problem for Estimation of Loads and Constraints from Structural Response Data

Sanjeev Padmanabhan* and Ashok V. Kumar†
University of Florida, Gainesville, Florida 32611-6300

DOI: 10.2514/1.17681

An important source of uncertainty in finite element models used for static and fatigue analysis is due to inaccuracy in estimating both the magnitude and distribution of loads. Furthermore, it is often assumed in the models that the structure is rigidly supported even though there may be significant compliance at the support. It is often difficult to accurately estimate the compliance as well as the actual distribution of the load. Recent improvements in experimental techniques enable full-field strain measurement with relative ease for structural components. A method for using these measurements to compute the applied load and distribution, as well as compliances at the supported boundaries, is presented in this paper. Accurately determining the loads and boundary conditions can significantly improve the ability to predict fatigue life and the likely location of failure for structures.

Nomenclature

E	=	error objective function
f_i	=	nodal force components
G_i	=	error in computed maximum shear strains
$\tilde{G}_j$	=	linear approximation of G_i
K_{ij}	=	stiffness matrix components
k_i	=	spring stiffness
N_k	=	shape functions
p	=	number of unknown force components
q	=	number of unknown spring compliances
T_{ij}	=	transformation matrix between local and global coordinates
U_i	=	error in computed displacements
$\tilde{U}_i$	=	linear approximation of U_i
u_i	=	computed displacement component
$\bar{u}_i$	=	measured displacement component
v_i	=	variables of the minimization problem
y_i	=	spring compliance
γ_j	=	computed in-plane maximum shear strain
$\bar{\gamma}_j$	=	measured in-plane maximum shear strain
ε_{kl}^{XYZ}	=	strain components with respect to global coordinates
ε_{ij}^{xyz}	=	strain components with respect to local coordinates xyz on the surface of the structure

I. Introduction

FOR critical load bearing structures, it is often necessary to perform finite element analysis to predict the stresses and fatigue life. However, the loads that a structure is subjected to during operation are sometimes difficult to estimate accurately. Furthermore, the distribution of the load may be nonuniform especially when the load is applied by contact between two structures. To create accurate models it is often necessary and desirable that the magnitude and distribution of the load be experimentally determined so that accurate finite element models can be developed for stress and fatigue life predictions. Another source of inaccuracy in finite element models is the applied boundary conditions. Because of difficulty in accurately estimating the compliance at the supports, it is common practice to assume that the supports are rigid. However, in many structural applications, such as shafts supported by rubber bushings, this is not a good assumption.

Strain measurement is routinely done during the design cycle of many products to ensure quality and reliability. Traditional techniques for strain measurement are point-measurements taken using strain transducers such as strain gauges. More recently, many full-field strain measurement techniques have evolved that are less intrusive and lower cost methods which provide continuous full-field measured data at high-spatial resolution. Examples of full-field measurement techniques include several optical measurement techniques [1,2] such as moiré interferometry [3,4], speckle methods [5,6], digital image correlation [7], and photoelastic [8] and brittle coatings [9]. Some of these measurement techniques provide displacement data, whereas others provide in-plane shear strain measurement. Unlike the traditional point-by-point measurement techniques, the full-field measurement techniques provide a very large data set even if the measurement is taken at only a fraction of the total surface area of the structure. Techniques that involve coating the surface with photoelastic materials often take measurements only at one conveniently accessible face of the structure.

The inverse method described in this paper was motivated by a full-field strain measurement technique that was developed by Hubner et al. [10–12] which makes use of a luminescent coating on a structure. This optical-based technique, called strain sensitive skin (S^3) is used to measure in-plane strain data on members under static loading conditions. This technique employs a coating consisting of a luminescent dye and polymer binder that is applied through aerosol techniques on the test member. Proper illumination stimulates the dye and makes it emit luminescence that has a different wavelength than the applied illumination. Optical filtering is used to separate the excitation and emission signals. Various calibration tests have shown that optical response is proportional to the sum of in-plane principal strains. This technique of measuring the strains makes it viable to determine strain fields for complex three-dimensional geometries. Furthermore, this luminescent coating technique enables strain data to be obtained at any point on the coated surface.

The goal of this paper is to present an inverse problem-solving technique to solve for the applied loads and support compliances, assuming that high-resolution displacement or shear strain data are available from a full-field measurement technique, and that a reasonably good finite element model of the structure is available. The stiffness of the structure computed by the finite element model is often not very accurate and could also be corrected or calibrated using the measured data, but no such attempt is made in this paper. It is also assumed that the surfaces or faces of the structure where loads are applied or the structure is supported are known. The load

Received 26 October 2005; revision received 2 February 2007; accepted for publication 5 February 2007. Copyright © 2007 by the American Institute of Aeronautics and Astronautics, Inc. All rights reserved. Copies of this paper may be made for personal or internal use, on condition that the copier pay the $10.00 per-copy fee to the Copyright Clearance Center, Inc., 222 Rosewood Drive, Danvers, MA 01923; include the code 0001-1452/07 $10.00 in correspondence with the CCC.

*Graduate Student, Mechanical and Aerospace Engineering, 237 MAE-B, University of Florida, Gainesville, FL.

†Associate Professor, Mechanical and Aerospace Engineering, 237 MAE-B, University of Florida, Gainesville, FL.

components at all the nodes on these loaded surfaces are treated as unknowns to be solved for in the inverse problem. Similarly, on the surfaces where the structure is supported, the compliance of the support is modeled as springs attached at all the nodes on the surface and the compliances of these are treated as unknowns to be solved for. Because a large amount of data are available from full-field measurement, the number of data points typically far exceed the number of unknowns. This allows the load distribution to be computed at significant high-resolution by having a dense mesh with a large number of nodes on the loaded surfaces.

Several methods have been developed for calculating the loads from the structural response data. Chock and Kapania [13] have described a method of updating the load by computing unknown coefficients of a polynomial used to represent the load distribution. The load is represented by Legendre polynomials with unknown weight factors. The weight factors are determined by minimizing the error between the measured values of displacements obtained experimentally and those found by finite element analysis. Shkarayev et al. [14] developed an inverse interpolation technique to determine loads based on parametric approximation of the aerodynamic loading. Cao et al. [15] demonstrated the use of artificial neural networks to identify loads distributed across a cantilevered beam. Carn and Trivailo [16] examined the use of neural networks to estimate the aerodynamic loading from structural response data. Aerodynamic loading conditions were simulated based on F/A-18 fatigue test data conducted by the Royal Australian Air Force. Liu et al. [17] have developed a video grammetric technique for determining aerodynamic loads. Optical elastic deformation measurements are used in their method to obtain the normal force and pitching moment.

Attempts have also been made to estimate structural stiffness or to identify similar system parameters using measured displacements and strains. Sanayei and Saletnik [18] have proposed a method to identify the element stiffness parameters of a structure by using elemental strain measurements. In a companion paper, Sanayei and Saletnik [19] described a heuristic approach for choosing a small subset of strain measurements to have least sensitivity to error in measurement. Truss and frame examples were used to demonstrate the aforementioned approach. The genetic algorithm (GA) approach has been used by Koh et al. [20] for parameter identification of large structural systems in the time domain. They proposed a modal GA method to overcome the enormous computational effort involved in a direct GA method. Reich and Park [21] have presented a theory for structural system identification using strains and translational displacements as measured outputs. The method proposed has been motivated by the advances in use of embedded piezoelectric sensors and fiber optics. Measured displacement data have been used to detect structural damage by probabilistic diagnosis concepts by Fu and Moosa [22]. They describe an optical method of using charge-coupled device cameras to measure the displacements in a loaded structure. The displacements are computed by subpixel edge detection techniques using images taken before and after the loads are applied.

The inverse method described here estimates loads and boundary conditions of a finite element model for a structure using displacement measurements, maximum in-plane shear strain measurements, or a combination of both types of data. A least-squares error function between the measured values and the corresponding values obtained by finite element analysis is minimized. The forces and compliance at the boundaries are treated as variables and the optimal values of these are computed. Section II describes the objective function to be minimized and describes a Gauss–Newton approach for minimizing the objective function. A method for efficiently computing the gradients of the objective function are also described in this section. Examples that were used to validate the algorithm are described in Sec. III. The examples include structures that are modeled using two- or three-dimensional finite element models. For validation purposes, structural response data computed using these models were used, instead of experimentally measured data, to compute the loads that were applied. Section IV provides the conclusions and discussion.

II. Optimization Method for Solving the Inverse Problem

Full-field measurements yield a large amount of data which can be used to update or correct the loads and boundary conditions of the model. Assuming that displacements, maximum shear strain, or a combination of the two are available at a sufficient number of points on the surface, an inverse problem can be solved to determine the loads and boundary conditions that would produce these displacements and strains. A least-squares minimization approach is used here to solve this inverse problem where the objective function is defined as the sum of the squares of the error between the displacements and strains obtained from the finite element analysis and the corresponding values measured experimentally. For the structure being modeled, it is assumed that the location of the application of the loads is known. Therefore, an initial guess for the loads are applied as nodal forces in the finite element model to specify the location where the loads are applied and the nonzero components of these applied nodal forces are treated as the unknown variables. Similarly, it is assumed that the region of the boundary of the structure that is supported by nonrigid (or compliant) fixtures is known. To model the compliances, springs are attached to the nodes at the location of the compliant supports and the compliances of these springs are treated as unknown variables to be solved for during the least-squares minimization. Up to three springs are attached at each node to represent the compliance in the x, y, and z directions. The objective function for the minimization can be written as

$$E(\boldsymbol{v}) = \sum_{i=1}^{m} U_i^2 + \sum_{j=1}^{l} G_j^2 \tag{1}$$

where

$$U_i = u_i - \bar{u}_i \qquad G_j = \gamma_j - \bar{\gamma}_j \tag{2}$$

It is assumed that m displacement data (components of displacement measured at many points) are available on the surface of the structure and that maximum shear strain is available at l points. The objective function is a function of the variables, denoted by the vector $\boldsymbol{v}$, which consists of the nodal force components and unknown spring compliances, whose components are inverse of the spring stiffness. The total number of unknowns is the sum of the number of unknown force components and spring compliances. The components of the vector $\boldsymbol{v}$ can therefore be defined as

$$v_i = \begin{cases} f_i & i \in [1, p] \\ y_i & i \in [p+1, p+q] \end{cases} \tag{3}$$

The errors U_i and G_j are in general nonlinear functions, therefore the objective function is not necessarily quadratic. However, if only displacement data are available and the unknowns are just the applied forces, then U_i are linear functions and the problem reduces to unconstrained quadratic programming. For the general case, we need to solve an unconstrained nonlinear optimization problem for computing the loads and compliances. The Gauss–Newton minimization approach is very efficient for solving least-squares minimization problems. At each iteration, the error functions are linearized at the current value of the variables so that the objective function becomes quadratic and can be solved by a single Newton iteration. If $\boldsymbol{v}^n$ is the value of the variable at the nth step of the iterations, then U_i and G_j are linearized as

$$\tilde{U}_i(\boldsymbol{v}) = U_i(\boldsymbol{v}^n) + \left.\frac{\partial U_i}{\partial v_r}\right|_n \Delta v_r \qquad \tilde{G}_j(\boldsymbol{v}) = G_j(\boldsymbol{v}^n) + \left.\frac{\partial G_j}{\partial v_r}\right|_n \Delta v_r \tag{4}$$

where Δv_r is a component of step vector $\Delta \boldsymbol{v} = \boldsymbol{v} - \boldsymbol{v}^n$ and there is an implied sum on the repeating index r. After substituting these linearized error functions into the objective function E, the optimality criteria for the resulting quadratic objective function is

$$\left(\frac{\partial U_i}{\partial v_s}U_i + \frac{\partial G_j}{\partial v_s}G_j\right) + \left(\frac{\partial U_i}{\partial v_s}\frac{\partial U_i}{\partial v_r} + \frac{\partial G_i}{\partial v_s}\frac{\partial G_i}{\partial v_r}\right)\Delta v_r = 0 \quad (5)$$

The preceding equation is linear in Δv_r and all the error functions and the derivatives in the equation are evaluated at $\boldsymbol{v} = \boldsymbol{v}^n$. There are implied sums on all repeating indices. The components of unknown variable vector $\boldsymbol{v}$ can be updated at $(n+1)$th step as

$$v_s^{n+1} = v_s^n + \Delta v_s \quad (6)$$

Both displacement and strain error computation require a finite element analysis, therefore, the gradients of these error functions, needed in Eq. (5), cannot be computed efficiently by finite difference approach. A sensitivity analysis using an adjoint variable method is required. The method for computation of the gradients is briefly discussed next. Based on Eq. (2), the gradients of the error functions U_i and G_j are the same as the gradients of the displacements and maximum shear strains, respectively. The displacements and maximum shear strains are functions of nodal forces $\boldsymbol{F}$ and the compliances $\boldsymbol{y}$.

$$u_i = u_i(\boldsymbol{f}, \boldsymbol{y}) \qquad \gamma_j = \gamma_j(\boldsymbol{u}) = \gamma[\boldsymbol{u}(\boldsymbol{f}, \boldsymbol{y})] \quad (7)$$

The displacements are computed by solving the system of linear equations generated by the finite element model

$$K_{ij}u_j = f_i \quad (8)$$

Taking the derivative of the Eq. (8) with respect to the force component f_s yields the following equation which can be solved to obtain the derivatives of displacements with respect to force components.

$$K_{ij}\frac{\partial u_j}{\partial f_s} = \delta_{is} \quad (9)$$

where, δ_{is} is the Kronecker delta. Solving the preceding equation yields the derivative of all the displacement components, whereas only a subset of these, corresponding to the points at which data are available, is needed for the computation of error.

The derivatives of the displacement with respect to spring stiffness can be computed by differentiating Eq. (8) with respect to the spring constants k_s.

$$K_{ij}\frac{\partial u_j}{\partial k_s} = -\frac{\partial K_{ij}}{\partial k_s}u_j \quad (10)$$

Solving the preceding equation gives the derivative of the displacement components with respect to spring stiffness which can be converted to derivative with respect to spring compliance using the relation between stiffness and compliance.

$$\frac{\partial u_i}{\partial y_s} = -k_s^2\frac{\partial u_i}{\partial k_s} \quad (11)$$

The maximum in-plane shear strains are computed at points on the surface of the structure using a local coordinate system xyz constructed such that the z axis is in the direction of the normal to the surface at those points. The normal direction (or z direction) is one of the principal directions of strain on any surface of a structure that does not have loads acting on it. Therefore, if the strain components are expressed with respect to this local coordinate system, then the maximum in-plane shear strain can be computed as

$$\gamma = \sqrt{\left(\frac{\varepsilon_{11}^{xyz} - \varepsilon_{22}^{xyz}}{2}\right)^2 + (\varepsilon_{12}^{xyz})^2} \quad (12)$$

The expressions for the derivatives of the maximum in-plane shear strain with respect to the unknown variable v_s can be obtained through chain rule differentiation.

$$\frac{\partial \gamma}{\partial v_s} = \frac{\partial \gamma}{\partial \varepsilon_{ij}^{xyz}}\frac{\partial \varepsilon_{ij}^{xyz}}{\partial \varepsilon_{kl}^{XYZ}}\frac{\partial \varepsilon_{kl}^{XYZ}}{\partial v_s} \quad (13)$$

The first term on the right hand side of the preceding equation can be computed by differentiating Eq. (12) with respect to each of the local strain components. The local strain components and the global strain components are related through a coordinate transformation matrix so that $\varepsilon_{ij}^{xyz} = T_{ki}\varepsilon_{kl}^{XYZ}T_{lj}$. Upon differentiating with respect to each global strain component, the second term in Eq. (13) can be computed as

$$\frac{\partial \varepsilon_{ij}^{xyz}}{\partial \varepsilon_{kl}^{XYZ}} = T_{ki}T_{lj} \quad (14)$$

In the finite element method, the global strain components at any point in an element are computed using the nodal displacements of the element. The relation between the nodal displacements and the strains is given as

$$\varepsilon_{ij}^{XYZ} = \frac{1}{2}\left(u_{ki}\frac{\partial N_k}{\partial x_j} + u_{kj}\frac{\partial N_k}{\partial x_i}\right) \quad (15)$$

where, u_{ij} is the jth displacement component of the ith node of an element and N_k are the shape functions of the element. The derivatives of strain with respect to the variables can be computed by differentiating Eq. (15) with respect to the unknown variable v_s.

$$\frac{\partial \varepsilon_{ij}^{XYZ}}{\partial v_s} = \frac{1}{2}\left(\frac{\partial u_{ki}}{\partial v_s}\frac{\partial N_k}{\partial x_j} + \frac{\partial u_{kj}}{\partial v_s}\frac{\partial N_k}{\partial x_i}\right) \quad (16)$$

The derivatives of the displacement with respect to the variables need to be computed first as described in Eqs. (9) and (11) and used in Eq. (16) to compute the derivatives of the strain components. Finally, substituting Eqs. (14) and (16) in Eq. (13), the derivatives of the maximum in-plane shear strains with respect to the unknown variables can be computed. Several iterations are needed for convergence when shear strain data are used. The magnitude of the gradient of the objective function divided by the number of data points is used for convergence checking.

III. Validation of the Algorithm

The optimization algorithm described in the previous section was implemented and incorporated into a finite element program. This software has been tested using several examples. In this section, four examples are provided to illustrate the capability of this method to determine the unknown forces and boundary conditions. In these examples, the algorithms are tested using structural response data that were generated either from analytical solutions or by finite element analysis results. The algorithm is validated by using these data to compute the loads. The computed load values are compared with the actual loads that were applied to generate the data to determine the accuracy of the method.

A. Beam Bending Under Linearly Varying Load

A cantilever beam problem with a known analytical solution is considered first to test the ability of the algorithm to determine the load distribution. Only displacement data generated using the analytical solution for deflection of the beam were used for this problem. Shear strain data were not used in this example. Figure 1 shows the beam with square cross section bending under the application of a linearly varying distributed load.

The deflection at any point along the beam can be computed from beam theory as

$$u = \frac{1}{EI}\left(\frac{-w_0x^4}{24} + \frac{w_0x^5}{120L} + \frac{w_0Lx^3}{18} - \frac{w_0L^3x}{45}\right) \quad (17)$$

The objective of this example is to demonstrate the ability of the algorithm to determine the load distribution on the beam when the deflection of the beam is known at a few points on the surface.

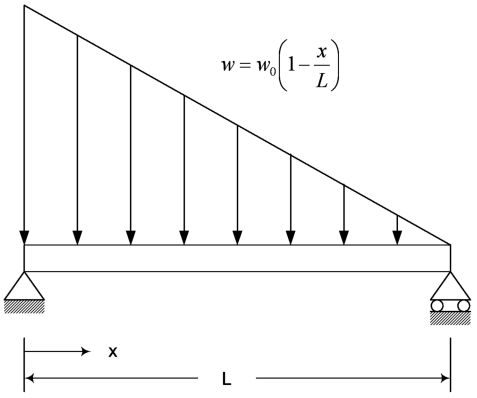

Fig. 1 Beam subjected to linearly varying load.

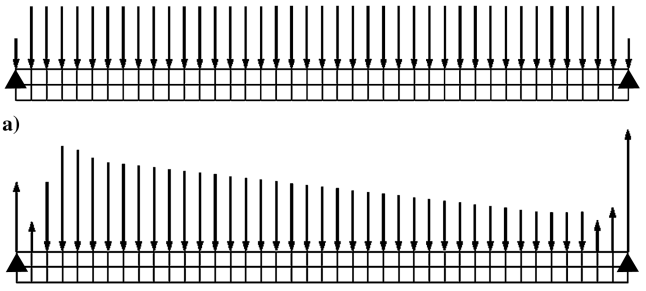

Fig. 2 Finite element mesh of simply supported beam with a) assumed loads, and b) computed loads.

Whereas the data were generated using analytical solution, the calibration is done using a two-dimensional plane stress finite element model which is incapable of reproducing the solution exactly equal to the analytical solution due to modeling errors, even if the exact value of the loads were known. This is similar to the situation when experimental data are used for the inverse problem, because the model used in the inverse algorithm is incapable of reproducing the experimental data exactly, even if the exact loads were known, due to modeling approximations.

The beam of length 1 m with a square cross section of side 5 cm was modeled as a plane stress problem using four node quad elements as shown in Fig. 2a. A linear load distribution was applied (see Fig. 1.) with $w_0 = 1000$ N/m. The material properties for the beam were assumed as 1) modulus of elasticity $E = 2.07 \times 10^{11}$ Pa, 2) Poisson's ratio $\nu = 0.29$, and 3) moment of inertia $I = 5.2083 \times 10^{-7}$ m^4.

The deflection along the beam was computed using Eq. (17) at 78 points and used as the structural response data. There are 41 unknown nodal forces acting on the top edge of the finite element mesh. An arbitrary load distribution can be applied on the beam as the initial values of the load at the start of the optimization iterations. In this example, a uniform load with a magnitude of 2000 N/m, as shown in Fig. 2a, was applied as the initial load. The load distribution was then computed by the error minimization algorithm using the displacement data obtained from the analytical solution. Figure 2b shows the computed nodal forces acting on the finite element mesh of the beam.

Figure 3 shows a plot of the analytical solution for deflection of the beam along with the deflections obtained from finite element analysis using both the initially assumed load and the deflections obtained using the computed nodal forces. As seen in the figure, the displacements obtained with the calibrated forces match very closely with the analytically computed displacements.

The nodal forces equivalent to the actual load distribution were computed by integrating the linearly varying load function. Figure 4 shows the nodal forces along the beam corresponding to the actual load (as assumed in the analytical model), as well as the initial load (uniform load) at the beginning of the iterations, and the nodal forces computed by the optimization process all in the same plot. It can be seen that the actual loading and the computed forces match very closely through most of the length of the beam. However, there are discrepancies at both ends of the beam. The beam has been modeled in the inverse problem algorithm as a plane stress problem. There are three nodes along the end face of the beam and only the middle node was fixed so that the beam could rotate about this node to simulate a pin joint. The concentrated reaction forces at these nodes produce stress concentrations so that the solutions at the end cannot match the analytical solution. Moreover, displacements computed using quadrilateral elements are not exact and will not match the analytical solution even if the exact loads used to compute the analytical solutions are applied. Despite these factors, a reasonably good estimate of the load is computed by the algorithm. The displacements computed by the plane stress finite element model using these computed loads closely match the analytical solution for displacement.

B. Three-Dimensional Bracket-Like Structure

In this example, a three-dimensional finite element model of a bracket-like structure is considered. The finite element mesh of the bracket shown in Fig. 5 consists of ten node tetrahedral elements. The right end of the bracket is clamped, whereas the top of the left end was

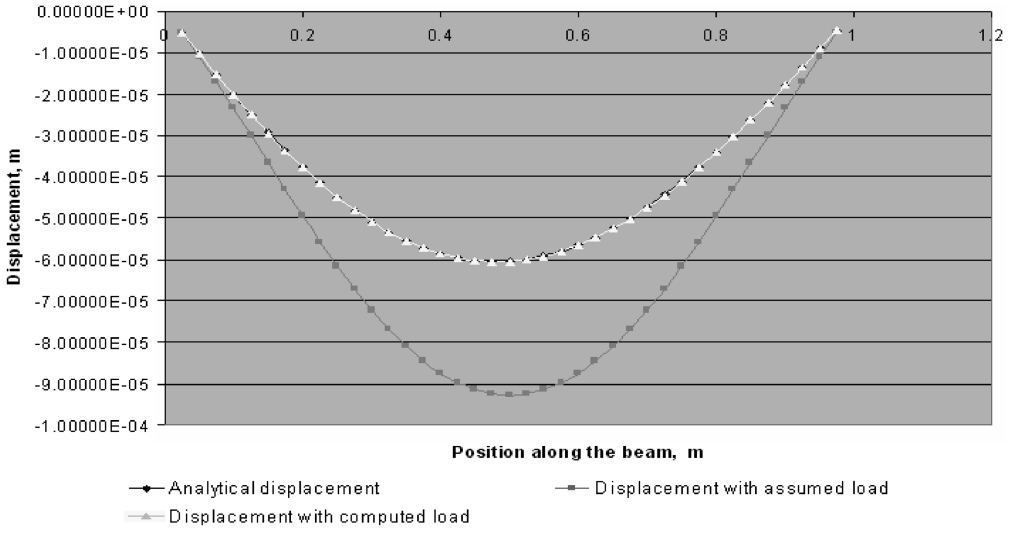

Fig. 3 Deflection along the length of the beam.

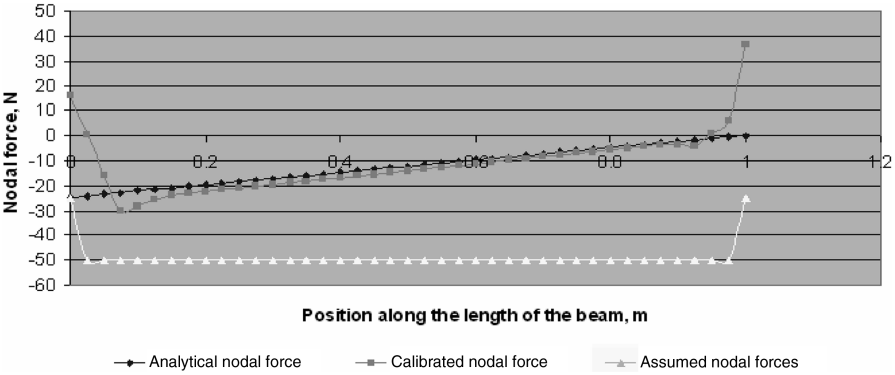

Fig. 4 Plot of analytical and computed nodal forces.

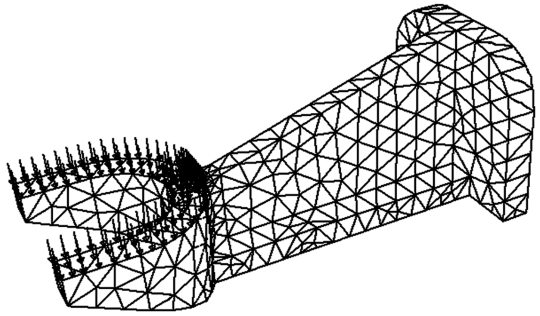

Fig. 5 Finite element model of the bracket.

subjected to a load distributed over the surface as shown. The material properties of the structure were defined as 1) modulus of elasticity $E = 2.07 \times 10^{11}$ Pa, and 2) Poisson's ratio $\nu = 0.29$.

To generate data for validating the algorithm, a total load of 1000 N was applied on the structure over 136 nodes as shown in Fig. 5 and a finite element analysis was performed. The displacements and maximum in-plane shear strains were computed only on the planar surfaces of the bracket and stored as data for subsequent validation of the inverse algorithm. A total of 446 shear strains and 2658 displacement components at points on the planar surfaces were used as the structural response data. In the inverse problem, it was assumed that the forces acting on the structure were unknowns and had to be computed. An arbitrary loading of 10,880 N was assumed as an initial guess for the applied load. The optimization algorithm was used to minimize the error between the recorded structural response data and the corresponding values from the finite element model, solving for the 136 unknown force variables.

Figures 6a and 6b show the displacement and von Mises stress contours obtained by finite element analysis when a load of 1000 N was applied for generating the structural response data. A gray scale pattern is used to display the values so that it can be better visualized in print. The minimum value is shown as black color which changes continuously through various shades of gray with the maximum value displayed as white. Figures 7a and 7b show the same values computed using the assumed initial loading of 10880 N. After computing the optimal load values using the minimization algorithm, these computed loads were applied on the same finite element mesh to compute the displacement results. The displacement magnitude and von Mises stresses obtained using the computed load are shown in Figs. 8a and 8b, respectively. Comparing the two results, it can be seen that displacements and stresses predicted by the computed loads in Fig. 8 are almost identical to those computed using the exact load in Fig. 6. The total load or the sum of the nodal forces computed was found to be 1000.0002 N which is almost exactly equal to the load that was applied to generate the data. Convergence was obtained after four iterations. The total CPU runtime was approximately 130 s on a personal computer. There is almost no error between the computed loads and the actual loads because the structural response data were obtained from the finite element analysis using the same mesh. In other words, the model used to generate the data is identical to the model used in the inverse problem. However, if experimental data are used or if the data are generated by a different model (such as an analytical solution), then it is unlikely that the computed forces will

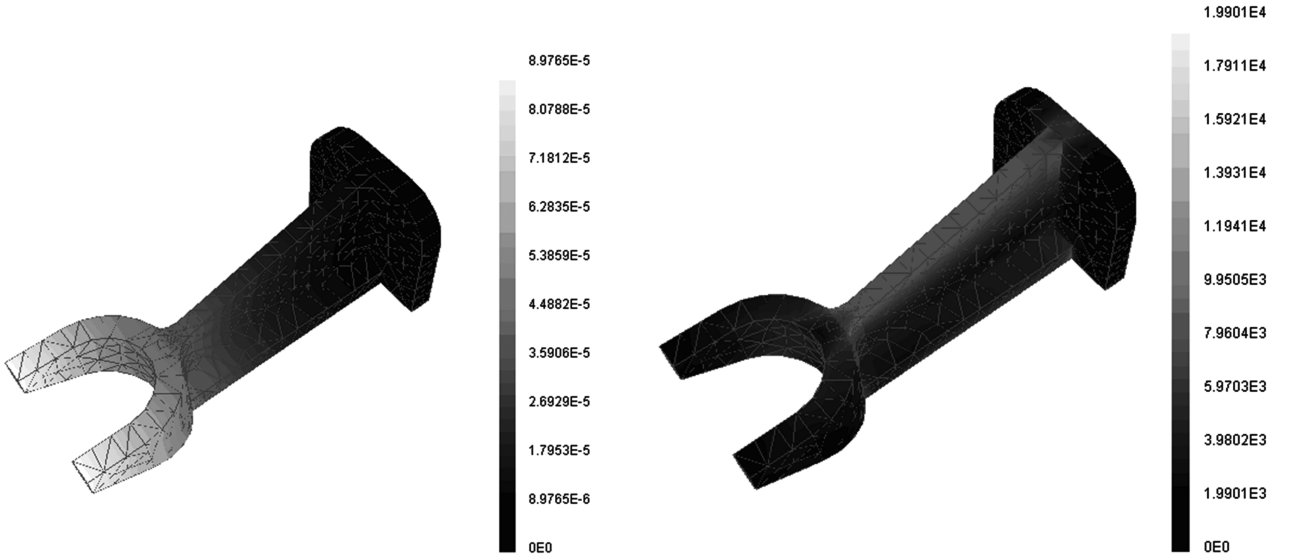

a) Displacement magnitude **b) Von Mises stress with actual loading**

Fig. 6 Results obtained by finite element analysis for a 1000 N load.

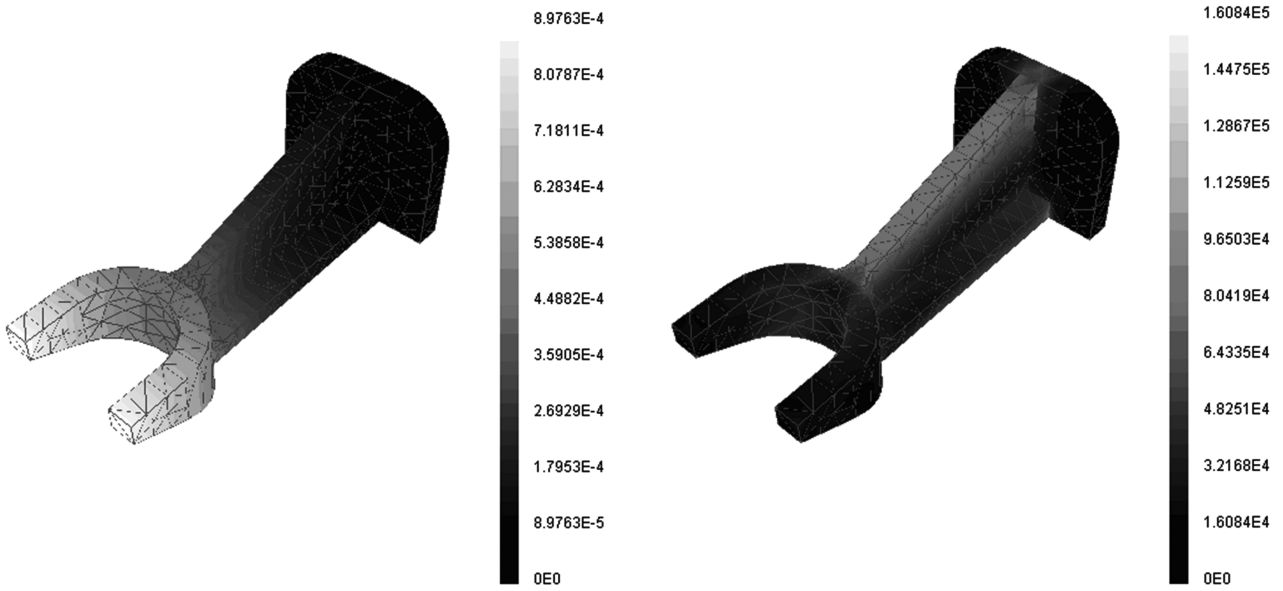

a) Displacement magnitude **b) Von Mises stress with assumed loading**

Fig. 7 Results obtained by finite element analysis with an assumed initial loading of 10,880 N.

exactly match the applied forces. The effect of errors in the data is studied in a later example.

C. Bracket with Unknown Loading and Boundary Conditions

A planar bracket that can be modeled as a plane stress problem is considered in this example to illustrate the capability of the optimization algorithm to estimate compliance at support boundaries. When a structure is supported by components in contact, whose compliances cannot be neglected, then the inverse problem algorithm can be used to determine these compliances. Figure 9 shows the bracket loaded with an unknown force at hole 1. The structure is supported by pins/bolts with compliant bushings through holes 2 and 3. To simulate the compliant supports, springs were attached at the nodes on the holes. Because this is a two-dimensional problem, two springs were attached at every node on holes 2 and 3 to simulate the compliance in the x and y directions. One end of the spring is fixed, whereas the other end is attached to a node. There were a total of 56 springs attached to the mesh.

The structure was modeled as a plane stress problem with quadrilateral elements with two-dimensional spring elements attached at all compliant supports. The material of the bracket was assumed to be steel with Young's modulus $E = 2.07 \times 10^{11}$ Pa and Poisson's ratio of 0.29. Again, to generate structural response data, finite element analysis was performed with all the spring constants set to $k_i = 5 \times 10^{14}$ N/m^2, $i = 1, 2, \ldots, 56$. The nodal forces applied at hole 1 for generating structural response data are listed in Table 1 under the column named actual nodal forces. The maximum in-plane shear strain at the midpoint of the elements and displacement at the nodes were computed by finite element analysis and used as structural response data.

In the inverse problem, the 14 nodal forces and the 56 spring compliances were treated as unknowns. The initial values for the spring stiffness were taken to be 2×10^{14} N/m^2. The actual nodal

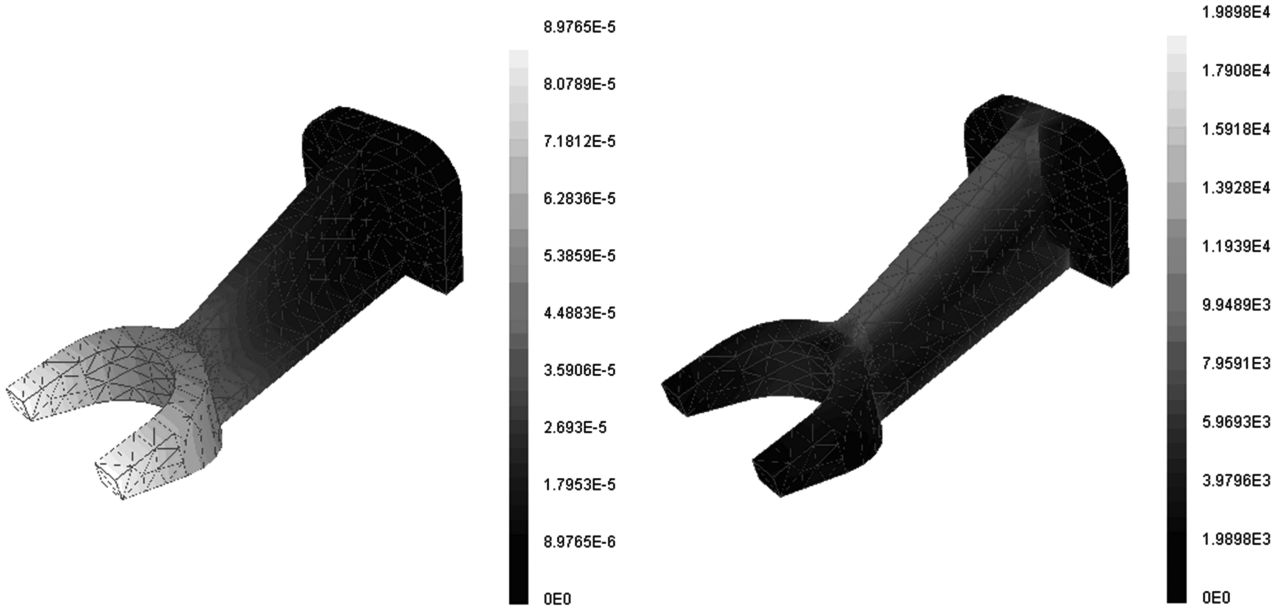

a) Displacement magnitude **b) Von Mises stress with computed loading**

Fig. 8 Results obtained by finite element analysis with computed loading.

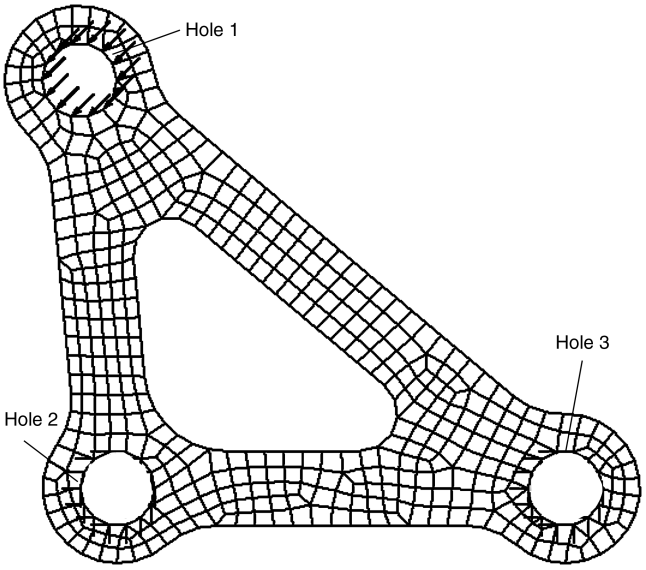

Fig. 9 Finite element mesh of the bracket.

forces and the forces computed by the optimization algorithm are shown in Table 1. Stiffness of all the springs was computed to be 5×10^{14} N/m^2. It was seen that even though the starting values of the forces and stiffness were arbitrary, almost the exact solution was obtained for forces and stiffness by solving the inverse problem in this example, again because the data was generated by the same model that was used in the inverse problem.

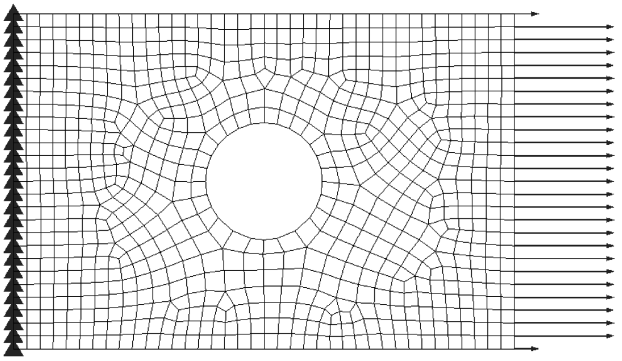

Fig. 10 Finite element mesh of plate with a circular hole.

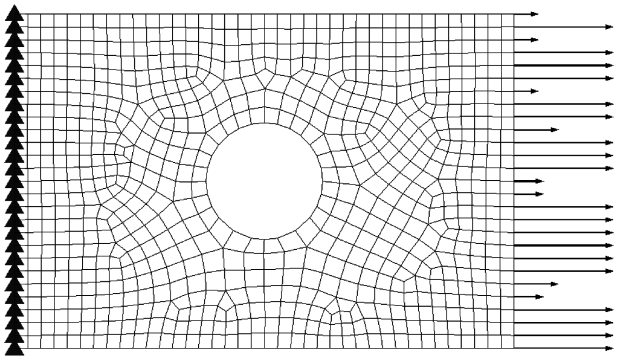

Fig. 11 Finite element mesh with assumed load.

D. Plate with Hole Example to Study Effect of Error in Data

In experimentally obtained data, there are typically errors associated with the measurements. As seen in previous examples, the forces and stiffness computed by the inverse problem can be exact if the data have no error and the model is capable of generating a solution that matches exactly with the data. In this example, a plate with a hole was modeled using plane stress elements to generate the structural response data and also for the inverse problem. To simulate the effect of measurement errors, arbitrary errors were added to data generated by finite element analysis with known loads. When both displacement and shear strain data are used for the calibration, as in the last two examples, it is not clear that both are contributing to the computed load. Therefore, in this example, only maximum shear stress data are used to show that the algorithm can compute the loads accurately even in the absence of displacement data.

Figure 10 shows the finite element model and the actual applied loads that were used to generate structural response data. In this example, a rectangular steel plate 6×4 in. with a circular hole of diameter 1.4 in. was axially loaded by a total load of 1000 lb applied uniformly at one end, while the other end of the plate was clamped as shown in Fig. 10. Only the maximum shear strain data were computed by finite element analysis and errors were added to the computed strain data before using it as structural response data. The error values were created using a random number generator after magnifying the random numbers to be equal to a specified percentage of the applied load. An arbitrary load (as shown in Fig. 11) was used as the initial load for the inverse problem. The sum of the nodal forces for this initial load was 1350 lb. The inverse problem was solved three times with different percentage errors (2, 5, and 10%) added to the strain data.

Figure 12 shows the plot of the actual nodal forces and the forces computed using 2, 5, and 10% error data. It is found that as the error in the data increases, the error in the values of individual nodal forces increase. However, the total load acting on the plate was estimated to be very close to the actual value. Table 2 lists the total loads obtained with each set of data.

Table 1 Force estimation for bracket problem

Node	Actual nodal force, N		Assumed nodal force, N		Computed nodal force, N	
	F_x	F_y	F_x	F_y	F_x	F_y
13	−50	−240	−500	−500	−50.0	−239.9
118	−100	−180	−500	−500	−99.9	−180.0
119	−500	−50	−500	−500	−500.0	−49.9
120	−800	−20	−500	−500	−799.9	−20.0
121	−890	−20	−500	−500	−889.9	−19.9
122	−993	−50	−500	−500	−993.0	−49.9
123	−995	−180	−500	−500	−994.9	−180.0
124	−1000	−240	−500	−500	−999.9	−239.9
125	−995	−270	−500	−500	−995.0	−269.9
126	−993	−290	−500	−500	−992.9	−290.0
127	−890	−300	−500	−500	−890.0	−299.9
128	−800	−300	−500	−500	−800.0	−299.9
129	−500	−290	−500	−500	−499.9	−290.0
130	−100	−270	−500	−500	−100.0	−269.9

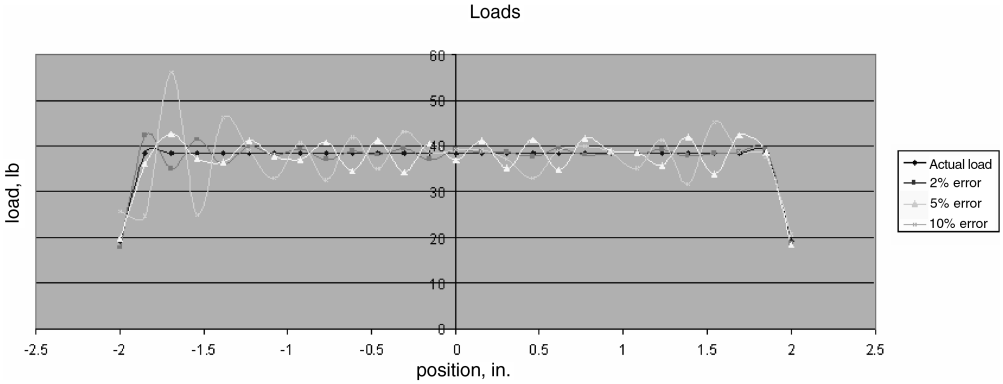

Fig. 12 Plot of actual and estimated loads.

The maximum value of shear strain near the stress concentration was 3.4876×10^{-6} with an axial load of 1000 lb. The maximum value of shear strain at the same location obtained with nodal forces computed with up to 2, 5, and 10% error in structural response is shown in Table 2. The errors in the maximum shear strain using the computed nodal forces are less than the errors in the structural response data that were used to compute these forces. This is due to the ability of least-squares minimization algorithms to filter out random errors very effectively. On the other hand, if the errors were biased to one side or the other that would have resulted in larger errors in the shear strain values obtained using the computed loads.

IV. Conclusions

An inverse problem approach for solving for applied loads and boundary conditions using observed response of the structure is presented. If experimental data of the structural response are available, either displacements or maximum shear strains, at enough points on the surface of the structure, then the method presented here can be used to compute applied loads and compliance at supports. Many experimental procedures, including the full-field strain measurement techniques, can often measure the structural response only at a portion of the surface of the structure. The algorithm presented here can then be used to estimate the applied loads and boundary conditions to update the finite element model so that reliable results can be obtained for the entire structure. The inverse problem is solved by a least-squares error minimization approach, where an error function constructed as the sum of squares of error between the predicted and measured data (strains/displacements) is minimized. Nodal forces or compliance of the springs attached at supports are solved by unconstrained minimization of the error function. Compliances of the springs were used as the variables instead of the stiffness of springs because the displacements are inversely proportional to stiffness and directly proportional to compliances. Therefore, the objective function is almost quadratic with respect to compliances, whereas it is an inversely related nonlinear function with respect to the stiffness of springs. The Gauss–Newton algorithm is able to minimize the objective functions efficiently when compliances of springs are used as the variables, whereas it often does not converge when stiffness of springs is used as the variables.

Table 2 Error estimate in computed loads

	Computed total load, lb	Error in load, %	Maximum value of shear strain	Error in maximum value of shear strain, %
Data with 2% error	1000.6	−0.06	3.4902×10^{-6}	−0.07
Data with 5% error	999.7	0.03	3.4843×10^{-6}	0.09
Data with 10% error	998.2	0.18	3.4790×10^{-6}	0.25

The examples presented here demonstrate that this technique is quite efficient and can reliably predict the unknown forces and boundary conditions. The results obtained are exact (but for numerical round-off errors) if the structural response data are generated using the same model that is used in the inverse problem. However, even if the data have random errors, the least-squares approach was found to yield results with a smaller percentage error for quantities, like the total load and the strains, away from the boundaries on which the load is applied. Modeling errors always exist and ensure that the values predicted by the model are never identical to experimental data even if the exact loads were known and the experimental data did not have any errors. However, as the first example in this paper showed, even when the model is unable to reproduce the data when the exact loads are applied, the algorithm is still able to compute a load distribution that is fairly close to the actual load, and the computed displacement using the computed load has even less error. Many previous papers have attempted to solve for concentrated loads or distributed loads that were parameterized to reduce the number of unknowns. The algorithm presented here is capable of computing load with higher resolution due to its ability to handle very large number of unknowns and to use very large data sets as obtained by full-field measurement techniques. The algorithms presented are being tested using experimental data obtained using luminescent photoelastic coatings [11] and will be published in a journal related to experimental mechanics.

Acknowledgments

The authors would like to thank James P. Hubner and Peter J. Ifju of the Mechanical and Aerospace Engineering Department, University of Florida and Wissam El-Ratal of Visteon Corporation for numerous discussions on experimental full-field strain measurement techniques that helped to define the problem.

References

[1] Daily, J. W., and Riley, W. F., *Experimental Stress Analysis*, 3rd ed., McGraw–Hill, New York, 1991.
[2] Cloud, G. L., *Optical Method of Engineering Analysis*, Cambridge Univ. Press, New York, 1998.
[3] Post, D., Han, B., and Ifju, P. G., *High Sensitivity Moire: Experimental Analysis for Mechanics and Materials*, Springer–Verlag, New York, 1994.
[4] Post, D., "Moire Interferometry," *Handbook on Experimental Mechanics*, edited by A. S. Kobayashi, Prentice Hall, Englewood Cliffs, NJ, 1987, Chap. 7.
[5] Stetson, K. A., "Review of Speckle Photography and Interferometry," *Optical Engineering*, Vol. 14, No. 5, 1975, pp. 482–489.
[6] Jones, R., and Wykes, C., *Holographic and Speckle Interferometry*, Cambridge Univ. Press, Cambridge, England, U.K., 1983.
[7] Peters, W. H., and Ranson, W. F., "Digital Imaging Techniques in Experimental Stress Analysis," *Optical Engineering*, Vol. 21, No. 3, 1982, pp. 427–432.
[8] Zandman, F., Redner, S., and Dally, J. W., *Photoelastic Coatings*, Iowa Press, Ames, IA, 1977.
[9] Durelli, A. J., Hall, J., and Stern, F., "Brittle Coating," *Handbook on*

Experimental Mechanics, edited by A. S. Kobayashi, Prentice Hall, Englewood Cliffs, NJ, 1987, pp. 516–554.
[10] Hubner, J. P., Ifju, P. G., Schanze, K. S., Jenkins, D. A., Carroll, B. F., Wang, Y., He, P., Brennan, A., and El-Ratal, W., "Full Field Strain Measurement Using a Luminescent Coating," *Experimental Mechanics*, Vol. 43, No. 1, 2003, pp. 61–68.
[11] Hubner, J. P., Ifju, P. G., Schanze, K. S., Liu, Y., Chen, L., and El-Ratal, W., "Luminescent Photoelastic Coatings," *Experimental Mechanics*, Vol. 44, No. 4, 2004, pp. 416–424.
[12] Hubner, J. P., Ifju, P. G., Schanze, K. S., Jaing, S., Liu, Y., and El-Ratal, W., "Luminescent Strain Sensitive Coatings," *44th AIAA/ASME/ASCE/AHS/ASC Structures, Structural Dynamics, and Materials Conference, Norfolk, Virginia*, AIAA Paper 2003-1437, 2003.
[13] Chock, J. M. K., and Kapania, R. K., "Load Updating for Finite Element Models," *AIAA Journal*, Vol. 41, No. 9, 2003, pp. 1667–1673.
[14] Shkarayev, S., Krashantisa, R., and Tessler, A., "Inverse Interpolation Method Utilizing In-Flight Strain Measurements for Determining Loads and Structural Response of Aerospace Vehicles," *3rd International Workshop on Structural Health Monitoring, September 12–14*, International Workshop on Structural Health Monitoring, Stanford, CA, 2001.
[15] Cao, X., Sugiyama, Y., and Mitsui, Y., "Application of Artificial Neural Networks to Load Identification," *Computers and Structures*, Vol. 69, No. 1, 1998, pp. 63–78.
[16] Carn, C., and Trivailo, P. M., "Inverse Determination of Aerodynamic Loading from Structural Response Data Using Neural Networks," *Inverse Problems in Science and Engineering*, Vol. 14, No. 4, 2006, pp. 379–395.
[17] Liu, T., Barrows, D. A., Burner, A. W., and Rhew, R. D., "Determining Aerodynamic Loads Based on Optical Deformation Measurements," *AIAA Journal*, Vol. 40, No. 6, 2001, pp. 1105–1112.
[18] Sanayei, M., and Saletnik, M. J., "Parameter Estimation of Structures from Static Strain Measurements 1: Formulation," *Journal of Structural Engineering*, Vol. 122, No. 5, 1996, pp. 555–562.
[19] Sanayei, M., and Saletnik, M. J., "Parameter Estimation of Structures from Static Strain Measurements 2: Error Sensitivity Analysis," *Journal of Structural Engineering*, Vol. 122, No. 5, 1996, pp. 563–572.
[20] Koh, C. G., Hong, B., and Liaw, C. Y., "Parameter Identification of Large Structural Systems in Time Domain," *Journal of Structural Engineering*, Vol. 126, No. 8, 2000, pp. 957–963.
[21] Reich, G. W., and Park, K. C., "Theory for Strain Based Structural System Identification," *Journal of Applied Mechanics*, Vol. 68, No. 7, 2001, pp. 521–527.
[22] Fu, G., and Moosa, A. G., "Optical Approach to Structural Displacement Measurement and its Application," *Journal of Engineering Mechanics*, Vol. 128, No. 5, 2002, pp. 511–520.

R. Kapania
Associate Editor

Aeronautics students, graduate students, and practicing engineers: Own the text that takes you beyond conceptual design of an aircraft and into the details of laying down the airframe…

Aircraft Loading and Structural Layout
Denis Howe

Denis Howe provides comprehensive coverage of all aspects of loading actions analysis together with the logical extension to the conceptual design of the airframe. He thereby meets two perceived needs that are not currently addressed by existing aircraft design texts: where loading analysis tends to be dealt with somewhat superficially, treating only the basic symmetric flight envelope; and where structural analysis often assumes that a certain level of design detail has already been established.

Readers will find a simple, logical sequence to derive the form, location, and approximate sizing of the main members of the airframe as a precursor to a comprehensive structural analysis and design refinement.

AIAA Education Series
2004, 591 pages, Hardback
ISBN: 1563477041
AIAA Member Price: $144.95
List Price: $199.95

Copublished with Professional Engineering Publishing. To order *or for more information, contact AIAA by phone: 800/682-2422, fax: 703/661-1595, e-mail:* warehouse@aiaa.org, *or online at* www.aiaa.org. For orders from Europe and the Middle East, please contact Professional Engineering Publishing, tel 44 1284 763 277 or fax 44 1284 704 006.

AIAA

05-0224